



Article

Numerical Study for the Effects of Temperature Dependent Viscosity Flow of Non-Newtonian Fluid with Double Stratification

Hafiz Abdul Wahab¹, Hussan Zeb^{1,2}, Saira Bhatti³, Muhammad Gulistan¹,
Seifedine Kadry^{4,*}  and Yunyoung Nam^{5,*} 

¹ Department of Mathematics & Statistics, Hazara University, Mansehra 21130, Pakistan; wahab@hu.edu.pk (H.A.W.); hussan.zeb@ovgu.de (H.Z.); Gulistanm21@yahoo.com (M.G.)

² Fakultät für Mathematik, Institute für Analysis Mathematik, OVGU, 39106 Magdeburg, Germany

³ Department of Mathematics, COMSATS University Islamabad, Abbottabad Campus, Abbottabad 22060, Pakistan; saira@cuiatd.edu.pk

⁴ Department of Mathematics and Computer Science, Faculty of Science, Beirut Arab University, Beirut 1107 2809, Lebanon

⁵ Department of Computer Science and Engineering, Soonchunhyang University, Asan 31538, Korea

* Correspondence: s.kadry@bau.edu.lb (S.K.); ynam@sch.ac.kr (Y.N.)

Received: 18 December 2019 ; Accepted: 13 January 2020; Published: 19 January 2020



Abstract: The main aim of the current study is to determine the effects of the temperature dependent viscosity and thermal conductivity on magnetohydrodynamics (MHD) flow of a non-Newtonian fluid over a nonlinear stretching sheet. The viscosity of the fluid depends on stratifications. Moreover, Powell–Eyring fluid is electrically conducted subject to a non-uniform applied magnetic field. Assume a small magnetic Reynolds number and boundary layer approximation are applied in the mathematical formulation. Zero nano-particles mass flux condition to the sheet is considered. The governing model is transformed into the system of nonlinear Ordinary Differential Equation (ODE) system by using suitable transformations so-called similarity transformation. In order to calculate the solution of the problem, we use the higher order convergence method, so-called shooting method followed by Runge-Kutta Fehlberg (RK45) method. The impacts of different physical parameters on velocity, temperature and concentration profiles are analyzed and discussed. The parameters of engineering interest, i.e., skin fraction, Nusselt and Sherwood numbers are studied numerically as well. We concluded that the velocity profile decreases by increasing the values of St , H and M . Also, we have analyzed the variation of temperature and concentration profiles for different physical parameters.

Keywords: variable viscosity and thermal conductivity; Eyring-Powell fluid; binary chemical reaction and activation energy; shooting method

1. Introduction

Nowadays the investigation of the MHD boundary layer behavior of different kind of fluids take a tremendous attraction due to its vast practical usage in industrial processes and engineering applications. These applications include petroleum industries, geothermal engineering, crystal growth, aerodynamics, nuclear reactors metallurgical processes, liquidating metals space technology, casting and spinning of fibers etc. In order to examine the rheological aspects of fluids, the Navier Stokes equations are insufficient alone. Therefore, rheological models are implemented to reduce this problem. The description of non-Newtonian fluids does not exist in single constitutive relationship between stress and strain. Few examples of non-Newtonian fluids are drilling mud, plastic

polymer, hot rolling, optical fibers, metal spinning, paper production and cooling of metallic plates. The investigation of the flow due to extending surface in a moving liquid is important in advanced industry, e.g., the expulsion of metals and plastics, glass blowing, cooling or drying of papers, etc. The problems of linear stretching sheet for many events of fluid have also been investigated by many number researchers; detail review for this article is explained as bellow.

Sakiadis [1] analyzed the boundary layer flow over a stretching surface. Various authors has been discussed the different feathers of the flow over a stretching surface. Vlegaar [2] studied the boundary layer on the stretching surface almost proportional to the distance from the orifice. Mahmood [3] et al. analyzed the un-uniform heat source or sink on MHD non-Darcian flow in a convective micropolar fluid over a stretching sheet with radiation. Crane et al. [4] evaluated the consequences of Newtonian fluid over a stretching sheet on the uniform stress. Haritha et al. [5] analyzed the effect of chemical reaction on convective boundary condition of a Maxwell fluid over a stretching surface in the appearance of thermal radiation. Zeb et al. [6] studied the effect of thermal radiation on time dependent fluid flow over a stretching sheet with variable thermal conductivity. Zeb et al. [7] studied the effect of thermal radiation and slip boundary condition on time dependent fluid flow over a stretching sheet along with variable thermal conductivity. Ghahderijani et al. [8] using the numerical solution of magnetohydrodynamics flow inside the Constricted Channels with local symmetric constrictions. Karimipour et al. [9] investigated the numerical solution of laminar MHD forced convection flow of carbon nanofluid in the microchannels with uniform heat flux. The combine effects of viscous dissipation and Heat transfer flow of pseudo-plastic nanofluid over a moving permeable surface with heat absorption/generation was studied by Maleki et al. [10]. The variation of thermal radiation on time dependent of a non-Newtonian Maxwell nanofluid over a stretching surface is carried out by Madhu et al. [11] via finite element method.

Magnetohydrodynamic (MHD) flow is the study of magnetic assets on electrically conducting fluids. Due to wide useful applications of MHD in industrial processes such as petroleum industries, plasma studies, manufacturing of heat exchangers, design for cooling of nuclear reactors, MHD power generator designing, and on the performance of many other processes. Soid et al. [12] was found the dual Solutions of time dependent flow over a shrinking sheet. Jamalabadi et al. [13] analyzed the formulation of subcooled boiling flow of nanofluid under the effect of a magnetic field. El-Dabe et al. [14] studied the characteristics of heat and mass transfer on MHD boundary layer flow of non-Newtonian fluid on a moving wedge. Khan et al. [15] also found the numerical assets on MHD laminar boundary layer flow past a wedge with the effects of, heat generation, thermal radiation and chemical reaction.

Another type of fluid is nano-fluids which is measured by dispersing of small sized materials such as nanotubes, nanofibers, nanowires, droplets, nanosheet and nanorods. The nano-fluids are nanoscale colloidal suspensions containing condensed nanomaterials. The productivity of polymerase chain reaction can be enhanced with the procedure of graphene based nano-fluid. Nanofluids require tunable optical assets, and due to these effects, they are used in solar collectors. Moreover nanofluids are also used in microfluids, biomedical, solid-state lighting, transportation, and manufacturing. The study of nano-fluids has been a topic of intense research during the last one decade due to their interesting thermophysical properties and anticipated applications in heat transfer. Angayarkanni et al. [16] evaluated the influence of particle size, volume fraction and particle morphology nanoparticles on the temperature dependent specific heat capacity of metal oxide nano-fluids via differential scanning calorimeter. Malvandi et al. [17] theoretical investigated the MHD mixed convective in a water nanofluid in a vertical annuler pipe. Nanofluid and heat transfer of water silver nano-particle inside a microchannel was studied numarically via finite element approach by Forghani et al. [18]. The numerical study of nanofluid flow over a streching sheet with heating joule effect was studied by Zeb et al. [19]. In the fluid suspensions, nano-materials have shown many exciting properties and the characteristic features present unparalleled potential, analyzed by Hua et al. [20]. Heat and mass transfer of a non-Newtonian fluid over a permeable surface with suction and injection effects

was calculated by Maleki et al. [21]. The extremely huge thermal conductivity can be report via inverse micellar templating and nanofiller. During melting and freezing the of the thermal features of n-hexadecane containing inverse micelles of volume fractions was studied by Philip et al. [22]. Lu et al. [23] evaluated the combined effects of non-linear radiation and zero mass flux surface on the axisymmetric steady carreau nano-fluid induced by a radially stretching sheet.

The Powell-Eyring has several advantages of using at low and high shear rates and can be reduced to Newtonian fluid by the derivation of kinetic theory of liquids. Hayat et al. [24] investigated the flow of Powell- Eyring model via asymptotic boundary condition through numerical approach. In last several decades the Powell-Eyring (PE) model got the attention of scientists in fluid dynamics due to its applications in both sciences and technological machinery. 3-D case of Powell- Eyring fluid past a stretching sheet was discussed by Palumbo et al. [25]. Also the evaluation of thermal radiation and convective boundary condition on Powell-Eyring fluid over a moving sheet was discussed by Akbar et al. [26]. Hayat et al. [27] calculated the effect of zero mass flux of nanoparticles on (MHD) flow of Powell–Eyring nanofluid toward a nonlinear stretching sheet. A numerical approach for the effect of Cattaneo–Christov heat flux model in MHD flow of Williamson fluid toward a stretching sheet with viscosity effects was found by Salahuddin et al. [28]. Hayat et al. [29] performed the investigation of Cattaneo—Christov heat flux in stagnation point flow of temperature dependent viscosity toward a nonlinear stretching sheet under the effect of double stratification.

Chemical reaction and thermal diffusion plays an important role on heat and mass transfer phenomena. The concentration difference produces qualitative and quantitative changes in the rate of heat transfer. Moreover, many chemically reacting processes consist of the species chemical reactions with finite Arrhenius activation energy. The phenomenon of Activation energy is mostly helpful in the fields of geothermal engineering or oil reservoir and in oil, water combinations. The relation between chemical reactions and mass transport are usually very difficult, and can be witnessed in the consumption and manufacturing of reactant species at different rates in fluid and mass transfer. Bestman [30] was published the boundary layer flow in heat and mass transfer under binary chemical reaction. The study of binary chemical reaction and activation energy was analyzed by Awad et al. [31] whose presented the solution via perturbation to shoe the effect of natural convection in a porous medium. The investigation of binary chemical reaction and activation energy on the time dependent rotating flow of heat and mass transfer was studied by Shafique et al. [32]. The effects of activation energy and binary chemical reactions was analyzed by [33–35].

Stratification depends upon on temperature, concentration differences or existence of fluids with different densities. Double stratifications play a vital role in engineering, industries, and sciences. The applications of stratifications include such as thermal stratification of reservoirs, processing rivers, oceans, manufacturing, different heterogeneous mixtures, ground water reservoirs, condensers of power plants, density stratification of atmosphere, etc. The biological processes occurring in reservoirs make the water in the bottom anoxic. The problem can be reduced with the implication of thermal stratification. Mukhopadhyay [36] was published a numerical study for double stratification on MHD heat and mass transfer fluid flow over exponential stretching surface along with suction and junction. The numerical aspects for the consequences of variable viscosity and dually stratification on Casson fluid toward a nonlinear stretching surface was studied by Animasaun et al. [37]. The effects of joule heating and thermal radiation on MHD flow of Cosson fluid due to nonlinear stretching sheet embedded by double stratifications was evaluated by Daniel et al. [38].

Previously, Khan et al. [39] analyzed a numerical approach change in viscosity of the Williamson nano-fluid flow over a nonlinear stretching sheet embedded in a double stratified medium. The viscosity depends on double stratification. The aims of current study is extend to the effects of change in viscosity and conductivity on Eyring Powell nano-fluid over a nonlinear stretching sheet along with chemical reaction and activation energy. Viscosity of the fluid depends on double stratification. We use similarity transformations for the transformation of governing model in to nonlinear coupled ordinary differential equation. We successfully compute the solution of this coupled

ordinary differential equation via numerical scheme (shooting method followed by Runge-Kutta Fehlberg method). The variations of different physical aspects are presented through graphs. Also, we obtained the numerical results of the local skin fraction, heat transfer rate and Sherwood number for various physical parameters through tables.

2. Mathematical Model

We have consider a mathematical model for MHD steady flow of change in viscosity on Eyring-Powell nano-fluid flow over a nonlinear stretching sheet along with double stratification. The flow is produced by a nonlinear stretching sheet. Moreover, the highlights of thermal conductivity and zero mass flux condition are taken into account. The sheet is stretched with velocity $u_w(x, y) = U_0(x + c)^{m-1}$, assume the sheet is designated with profile $y = A(x + c)^{\frac{m-1}{2}}$ here U_0 stretching rate, c dimensionless constant, A represents constant, m represents stretching index. Moreover, it is supposed that the model needs to be satisfied individual for $m \neq 1$, because for $m = 1$, it decreases to flat surface. A magnetic field B_o is applied normal to the sheet, vertical to the surface (see in Figure 1). The assumption of rate process is used to obtained the Eyring Powell model (1994) in order to explain the shear of non-Newtonian flow. Akber et al. [26] evaluated the shear stress of in Eyring Powell model as

$$\tau_{i,j} = \mu \frac{\partial \hat{u}_i}{\partial \hat{u}_j} + \frac{1}{\beta_1} \sinh^{-1} \left(\frac{1 \partial \hat{u}_i}{c \partial \hat{u}_j} \right) \tag{1}$$

here μ represents the dynamic viscosity, c and β_1 are represents parameters of the fluid. We take the second order approximation as

$$\sinh^{-1} \left(\frac{1 \partial \hat{u}_i}{c \partial \hat{u}_j} \right) \cong \left(\frac{1 \partial \hat{u}_i}{c \partial \hat{u}_j} \right) - \frac{1}{6} \left(\frac{1 \partial \hat{u}_i}{c \partial \hat{u}_j} \right)^3 \tag{2}$$

Under the above assumptions and boundary layer approximation leads to the governing expressions [26,37–39] (Eyring Powell nano-fluid model, energy and concentration formulation) are stated from operation (3)–(6) as follows:

$$\frac{\partial \hat{u}}{\partial x} + \frac{\partial \hat{v}}{\partial y} = 0, \tag{3}$$

$$\hat{u} \frac{\partial \hat{u}}{\partial x} + \hat{v} \frac{\partial \hat{u}}{\partial y} = \frac{\partial}{\partial y} (\mu(T) \frac{\partial \hat{u}}{\partial y}) + \frac{1}{\rho \delta c} \frac{\partial^2 \hat{u}}{\partial y^2} - \frac{1}{2 \rho \delta c^3} \left(\frac{\partial \hat{u}}{\partial y} \right)^2 \left(\frac{\partial^2 \hat{u}}{\partial y^2} \right) - \sigma \frac{B_0^2 \hat{u}}{\rho}, \tag{4}$$

$$\hat{u} \frac{\partial \hat{T}}{\partial x} + \hat{v} \frac{\partial \hat{T}}{\partial y} = \frac{\partial}{\partial y} \left(k(\hat{T}) \frac{\partial \hat{T}}{\partial y} \right) + \tau \left[\left(\frac{D_{\hat{T}}}{\hat{T}_{\infty}} \right) \left(\frac{\partial \hat{T}}{\partial y} \right)^2 + D_B \left(\frac{\partial C}{\partial y} \frac{\partial \hat{T}}{\partial y} \right) \right] \tag{5}$$

$$\hat{u} \frac{\partial C}{\partial x} + \hat{v} \frac{\partial C}{\partial y} = D_B \left(\frac{\partial^2 C}{\partial y^2} \right) + \tau \left(\frac{D_{\hat{T}}}{\hat{T}_{\infty}} \right) \left(\frac{\partial^2 \hat{T}}{\partial y^2} \right) - k_r \left(\frac{\hat{T}}{\hat{T}_{\infty}} \right)^n \exp \left(\frac{-E}{\zeta \hat{T}} \right) (C - C_{\infty}). \tag{6}$$

Subjected to boundary condition

$$\hat{u}(x, y) = \hat{u}_w(x) = U_0(x + c)^m, \quad \hat{v}(x, y) = 0 \tag{7}$$

$$\hat{T}(x, y) = \hat{T}_w(x, y) + N \frac{\partial \hat{T}}{\partial y},$$

$$\left(D_B \frac{\partial C}{\partial y} \right) + \left(\frac{D_{\hat{T}}}{\hat{T}_{\infty}} \right) \left(\frac{\partial \hat{T}}{\partial y} \right) = 0, \quad \text{at } y = A(x + c)^{\frac{1-m}{2}}, \tag{8}$$

$$\hat{u}(x, y) \rightarrow 0, \quad \hat{T} \rightarrow \hat{T}_{\infty} \quad C \rightarrow C_{\infty} \quad \text{as } y \rightarrow \infty. \tag{9}$$

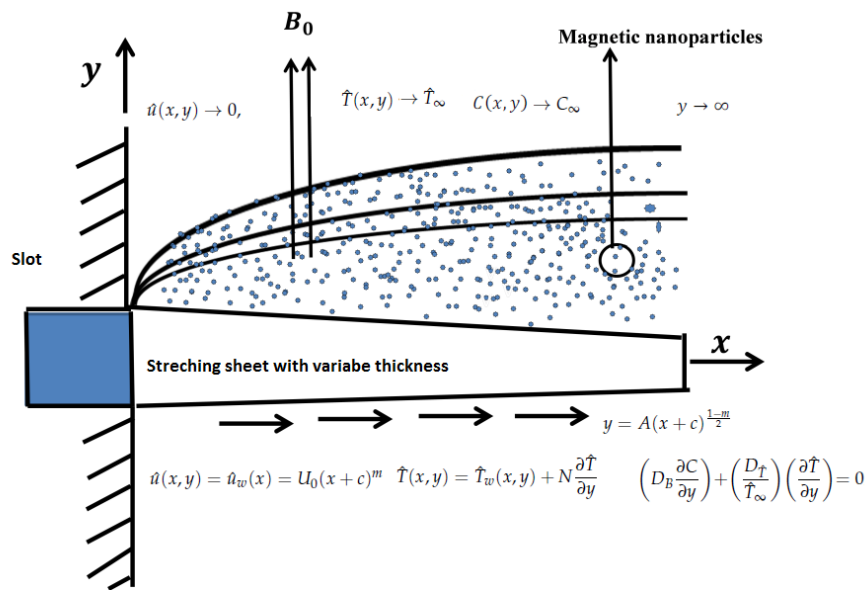


Figure 1. Geometry of the problem.

In the above expression the velocity components \hat{u} and \hat{v} are in the x and y - directions, respectively, $\mu(T)$ denotes viscosity, ρ the density of the nanoparticle, \hat{T} denotes the temperature of the nanofluid, \hat{C} represent the concentration of the nanofluid, C_w and \hat{T}_w the concentration and temperature and along the stretching sheet. \hat{C}_∞ and \hat{T}_∞ the ambient concentration and temperature, $(\rho c)_f$ the heat capacitance of the base fluid, $D_{\hat{T}}$ the thermosteresis coefficient. The Arrhenius law in Equation (6) was obtained by Arrhenius [40], $(\frac{\hat{T}}{\hat{T}_\infty})^n \exp(\frac{-E}{\zeta \hat{T}})(\hat{C} - \hat{C}_\infty)$ represents the modified form of Arrhenius function in which $\zeta = 8.61 \times 10^{-5}$ eV denotes the Boltzmann constant, n is the unit less exponent fitted rate constant typically lies in range $-1 < n < 1$ and E represents the activation energy. The variation in viscosity and thermal conductivity due to internal friction between the stretching surface and fluid paretical have to be taken into account, it is appropriate to assumed the mathematical formulation of the thermal conductivity and viscosity depends on temperature was investigated in [37–39] together with useful similarity variables as follows:

$$\begin{aligned} \mu(\hat{T}) &= \check{\mu}(a + b_1(\hat{T}_w - \hat{T})), & k(\hat{T}) &= \check{\mu}(a_1 + b_2(\hat{T} - \hat{T}_\infty)), \\ \theta(\zeta) &= \frac{\hat{T} - \hat{T}_\infty}{\hat{T}_w - \hat{T}_\infty}, & \phi(\zeta) &= \frac{C - C_\infty}{C_w - C_\infty} \end{aligned} \tag{10}$$

Transform governing model into ODEs by using following similarity variable as follows:

$$\begin{aligned} \hat{T}_w &= \hat{T}_0 + n_1(x+c)^{\frac{1-m}{2}}, & \hat{T}_\infty &= \hat{T}_0 + n_2(x+c)^{\frac{1-m}{2}}, \\ \hat{C}_w &= \hat{C}_0 + n_3(x+c)^{\frac{1-m}{2}}, & \hat{C}_\infty &= \hat{C}_0 + n_4(x+c)^{\frac{1-m}{2}}. \end{aligned} \tag{11}$$

Using Equation (11) we obtained

$$\begin{aligned} \hat{T}_w - \hat{T} &= (1 - \theta)\hat{T}_w - \hat{T}_0 - n_2(x+c)^{\frac{1-m}{2}} \\ \hat{C}_w - \hat{C} &= (1 - \phi)\hat{C}_w - \hat{C}_0 - n_4(x+c)^{\frac{1-m}{2}} \end{aligned} \tag{12}$$

From Equations (10) and (11) can easily obtained as follows

$$\begin{aligned} b_1(\hat{T}_w - \hat{T}_0) &= b_1 n_1(x+c)^{\frac{1-m}{2}}, & b_1(\hat{T}_\infty - \hat{T}_0) &= b_1 n_2(x+c)^{\frac{1-m}{2}} \\ b_2(\hat{C}_w - \hat{C}_0) &= b_3 n_1(x+c)^{\frac{1-m}{2}}, & b_2(\hat{C}_\infty - \hat{C}_0) &= b_4 n_2(x+c)^{\frac{1-m}{2}} \end{aligned} \tag{13}$$

in the above expression \hat{T}_o and \hat{C}_o are reference temperature and concentration respectively. Form Equation (13) we obtained

$$b_1(\hat{T}_w - \hat{T}_o) = d, \quad b_1(\hat{T}_\infty - \hat{T}_o) = dSt, \quad St = \frac{n_2}{n_1},$$

$$b_2(\hat{C}_w - \hat{C}_o) = d, \quad b_2(\hat{C}_\infty - \hat{C}_o) = dSc, \quad Sc = \frac{n_4}{n_3}, \tag{14}$$

$$\varepsilon = b_2(\hat{T}_\infty - \hat{T}_o) \quad \varepsilon St = b_2(\hat{T}_w - \hat{T}_o) \tag{15}$$

Introducing the following similarity transformations

$$\zeta = \sqrt{\frac{(m-1)U_o(x-c)^{(m-1)}}{2v}}y, \quad \psi = \sqrt{\frac{2vU_o(x-c)^{(m+1)}}{m+1}}F(\zeta), \tag{16}$$

$$\hat{u} = U_o(x+c)^m F'(\zeta), \quad \Theta(\zeta) = \frac{T - T_w}{T_w - T_\infty}, \quad \Phi(\zeta) = \frac{C - C_w}{C_w - C_\infty} \tag{17}$$

$$\hat{v} = \sqrt{\frac{(m-1)vU_o(x-c)^{(m-1)}}{2}}[F(\zeta) + \zeta \frac{m-1}{m+1}F'(\zeta)], \tag{18}$$

by substituting the above similarity transformation Equations (3)–(6) reduces into the following system of ODEs:

$$(a + d(1 - \Theta - St))F''' - \frac{(m+1)}{2}H\lambda F'''(F'')^2 - d\Theta'F'' + FF'' - \frac{2m}{m+1}F'^2 - \frac{2M}{m+1}F' = 0, \tag{19}$$

$$\frac{a_1 + \varepsilon\Theta}{Pr}\Theta'' - \frac{m-1}{m+1}\Theta F' - St \frac{m-1}{m+1}F' - F\Theta' + \frac{\varepsilon}{Pr}\Theta^2 + Nb\Phi'\Theta' + Nt(\Theta')^2 = 0, \tag{20}$$

$$\frac{\Phi''}{PrLe} - \frac{m-1}{m+1}\Phi F' - Sc \frac{m-1}{m+1}F' + \frac{N_b}{PrLeN_t}(\Theta'') - F\Phi' - Kr((1 + \delta\Theta)^n \exp(\frac{-E}{(1 + \delta\Theta)}))\Phi = 0. \tag{21}$$

Subject to boundary condition

$$F(\zeta) + \alpha \frac{m-1}{m+1}F' = 0, \quad \Theta(\alpha) = 1 + Lt\Theta'(\alpha), \quad F'(\alpha) = 1 \quad Nb\Phi'(\alpha) + Nt\Theta'(\alpha) = 0, \quad \alpha = 0. \tag{22}$$

$$F'(\alpha) = 0, \quad \Theta(\alpha) = 0, \quad \Phi(\alpha) = 0, \quad \text{at } \alpha \rightarrow \infty.$$

Further more considring $F(\eta) = f(\zeta - \alpha) = f(\eta)$, $\Theta(\eta) = \theta(\zeta - \alpha) = \theta(\eta)$ ans $\Phi(\eta) = \phi(\zeta - \alpha) = \phi(\eta)$, Equations (19)–(21) with boundary conditions 22 as follows:

$$(a + d - d\theta - Std)f''' - d\theta'f'' - \frac{(m+1)}{2}H\lambda f'''(f'')^2 + ff'' - \frac{2m}{m+1}f'^2 - \frac{2M}{m+1}f' = 0, \tag{23}$$

$$\frac{a_1 + \varepsilon\theta}{Pr}\theta'' - \frac{m-1}{m+1}\theta f' - St \frac{m-1}{m+1}f' - f\theta' + \frac{\varepsilon}{Pr}\theta^2 + Nb\phi'\theta' + Nt(\theta')^2 = 0, \tag{24}$$

$$\frac{\phi''}{PrLe} - \frac{m-1}{m+1}\phi f' - Sc \frac{m-1}{m+1}f' - f\phi' + \frac{N(b)}{PrLeN_t}(\theta'') - Kr((1 + \delta\theta)^n \exp(\frac{-E}{(1 + \delta\theta)}))\phi = 0. \tag{25}$$

Subject to boundary condition

$$f(\eta) + \alpha \frac{m-1}{m+1}f' = 0, \quad f'(\eta) = 1, \theta(\eta) = 1 + Lt\theta'(\eta), \quad Nb\phi'(\eta) + Nt\theta'(\eta) = 0, \quad \eta = 0. \tag{26}$$

$$f'(\eta) = 0, \quad \theta(\eta) = 0, \quad \phi(\eta) = 0, \quad \text{at } \eta \rightarrow \infty. \tag{27}$$

where f' is the dimensionless velocity, θ denotes the temperature, ϕ represents the concentration η denotes the similarity variables where $M = \frac{\sigma(B_o)^2}{\rho U_o(x+c)^{m-1}}$ is magnetic parameter, $\alpha = A((\frac{U_o(1+m)}{2v}))^{1/2}$ represents the wall thickness parameter, $Pr = \frac{\mu C_p}{k_\infty}$ is Prandtl number, $Re_y = \frac{u_w \sqrt{y}}{\nu}$ Reynolds number,

$H = \frac{1}{\mu\beta_{1c}}$ and $\lambda = \frac{\rho u_w}{2xc^2\mu}$ are fluid parameters. $Nb = \frac{\tau D_B}{\nu}(\hat{T}_w - \hat{T}_\infty)$ the Brownian motion parameter, $Le = \frac{\nu}{D_b}$ the Lewis number, $K_r = \frac{k_0}{b}$ the reaction rate parameter, $Nb = \frac{\tau D_B}{\nu}(\hat{C}_w - \hat{T}_\infty)$ the Brownian motion parameter, $E = \frac{E_a}{\zeta C_\infty}$, denotes activation energy, $\delta = \frac{\hat{T}_w - \hat{T}_\infty}{\hat{T}_\infty}$ represents temperature relative parameter. The quantities C_g , $Nu_{\hat{x}}$ and $Sh_{\hat{x}}$ are define by

$$C_f = \frac{\tau_w}{\rho u_w^2}, \tag{28}$$

$$Nu_x = \frac{xq_w}{k(\hat{T}_w - \hat{T}_\infty)}, \tag{29}$$

$$Sh_x = \frac{xq_m}{D_B(C_w - C_\infty)}, \tag{30}$$

where τ_w represents the skin friction along the stretching surface, q_w the heat flux and j_m the concentration flux from the surface and are given by

$$\tau_x = \mu(\hat{T}) \left[\left(1 + \frac{1}{\beta c}\right) \frac{\partial \hat{u}}{\partial y} + \frac{1}{\beta c^6} \left(\frac{\partial \hat{u}}{\partial y}\right)^3 \right]_{y=0} \quad q_w = \left[-k \frac{\partial \hat{T}}{\partial y}\right]_{y=0} \quad j_m = \left[-D_B \frac{\partial C}{\partial y}\right]_{y=0}, \tag{31}$$

where u_w , q_m and q_w , represents the wall shear stress, mass flux and heat transfer respectively. The skin fraction, local Nusselt and Sherwood numbers are transform in dimensionless form as follows

$$C_f \sqrt{Re_x} = (a + d - d\theta - Std) \left(\sqrt{\frac{m-1}{2}} (1+H) f''(0) - \sqrt{\frac{m-1}{2}} \frac{H\lambda}{3} (f''(0))^3 \right), \tag{32}$$

$$\frac{Nu_x}{\sqrt{Re_x}} = -\sqrt{\frac{m-1}{2}} \left[1 + \varepsilon\theta(0) \right] \theta'(0), \quad \frac{Sh_x}{\sqrt{Re_x}} = -\sqrt{\frac{m-1}{2}} \phi'(0).$$

3. Numerical Method

Equations (19)–(21) are the system of nonlinear, 3rd order in f , 2nd order in θ and 2nd order in ϕ respectively. First of all these non-linear ODE's are reduce into a system of first order ODE's and then solved by using shooting method. The Equations (19)–(21) can be written as:

$$f''' = - \left[\frac{-d\theta' f'' + f f'' - \frac{2m}{m+1} f^2 - \frac{2}{m+1} M f'}{a + d - d\theta - Std + H - 0.5(m+)H\lambda (f'')^2} \right], \tag{33}$$

$$\theta'' = - \frac{Pr}{a_1 + \varepsilon\theta} \left[-\frac{m-1}{m+1} \theta f' - St \frac{m-1}{m+1} f' - f\theta' + \frac{\varepsilon}{Pr} \theta^2 + Nb\phi'\theta' + Nt(\theta')^2 \right], \tag{34}$$

$$\phi'' = -LePr \left[\frac{m-1}{m+1} \phi f' - Sc \frac{m-1}{m+1} f' - f\phi' - Kr((1 + \delta\theta)^n \exp(\frac{-E}{(1 + \delta\theta)})\phi) \right] - \frac{N_b}{N_t} (\theta'') \tag{35}$$

To convert these higher order nonlinear ODE's into system of first order ODE's, let

$$f = u_1, \quad f' = u_2, \quad f'' = u_3 \quad \text{and} \quad f''' = u'_3, \tag{36}$$

$$\theta = u_4, \quad \theta' = u_5 \quad \text{and} \quad \theta'' = u'_5 \tag{37}$$

$$\phi = u_6, \quad \phi' = u_7 \quad \text{and} \quad \phi'' = u'_7 \tag{38}$$

The nonlinear coupled ODE's are converted into a system o first order simultaneous algebraic form, which can be defined as form as

$$u'_1 = u_2, \tag{39}$$

$$u'_2 = u_3, \tag{40}$$

$$u'_3 = - \left[\frac{-du_5u_3 + u_1u_3 - \frac{2m}{m+1}u_2^2 - \frac{2}{m+1}Mu_2}{a + d - du_4 - Std + H - 0.5(m+)H\lambda(u_3)^2} \right], \tag{41}$$

$$u'_4 = u_5, \tag{42}$$

$$u'_5 = - \frac{Pr}{a_1 + \epsilon u_4} \left[- \frac{m-1}{m+1}u_4u_2 + \frac{\epsilon}{Pr}u_5^2 - St \frac{m-1}{m+1}u_2 + u_1u_5 + Nbu_7u_5 + Nt(u_5)^2 \right] \tag{43}$$

$$u'_6 = u_7, \tag{44}$$

$$u'_7 = -LePr \left[u_7u_1 - \frac{m-1}{m+1}u_6u_2 - Sc \frac{m-1}{m+1}u_2 - Kr((1 + \delta u_4)^n \exp(\frac{-E}{(1 + \delta u_4)})u_6) \right] - \frac{N_b}{N_t}(u'_5).$$

boundary conditions are

$$u_1(0) + \alpha \frac{m-1}{m+1}u_2(0) = 0, \quad u_2(0) = 1, \quad u_4(0) = 1 + Ltu_4(0), \quad Nbu_6(0) + Ntu_4(0) = 0, \tag{45}$$

$$u_2(\infty) = 0, \quad u_4(\infty) = 0, \quad u_6(\infty) = 0 \tag{46}$$

To determine the solution of system of seven ODE's (39)–(45) by using shooting method, seven initial assumptions are required, but in system (46) two initial guesses are given in f one in θ and one in ϕ and the other three conditions are defined as $\eta \rightarrow \infty$. These three conditions generate result in three unknowns. The subsequent and foremost step of this method is choosing the estimated values of η at ∞ , solution process is initiated with certain initial guesses and finding out the solution of (BVP) including governing model. The method of solution with a new values of η at $\eta \rightarrow \infty$ and the method is repeated until two consecutive values of $f''(0)$, $\theta'(0)$ and $\phi'(0)$ are different only after the significant digits. Thus final values of η is considered as $\eta \rightarrow \infty$.

4. Results and Discussions

The system of the governing Equations (19)–(21) are solved numerically by using shooting method. We have taken $\Delta(\eta) = 0.02$ also the boundary condition ∞ has been replaced with 5 due to the requirement of the shooting method. The convergence has been obtained at $\text{tol } \epsilon = 10^{-5}$, while the thickness of the boundary layer η_∞ is taken between 2 and 15. Moreover the current result is compared with previously published data see in Table 1. The variation of different physical aspects are presented through graphs (as shown in Figures 2–23). The distribution of horizontal velocity on (thermal stratification) shown in Figure 2. It is viewed that the velocity gradient reduces by enlarging values of St . Figure 3 is sketches for the distribution temperature gradient for unlike values of St . It is clear that temperature gradient increases for higher values of St . Plotted Figure 4 is for the variation of velocity and temperature distribution for unlike values of M . Decrease variation of velocity and temperature profiles increases by enlarge values of M . According to the Lorentz's force theory, the behavior of magnetic field and velocity fraction is inverse. Therefore the velocity distribution is reduced by the higher values of M . Plotted Figure 5 is plotted for the distribution of concentration and temperature profiles for the distinct values of (Prandtl number Pr). The temperature profile decreases and concentration profile increases by increasing values of Pr . The physical reason behind that the fluids contain a little number of Pr have a higher thermal diffusivity, and this behaviour is inverse for larger values of Prandtl numbers. Figure 6 indicates that the significance of velocity for various values of material fluid parameter H . By increasing H the velocity decreases, hence velocity and momentum boundary layer thickness are increased.

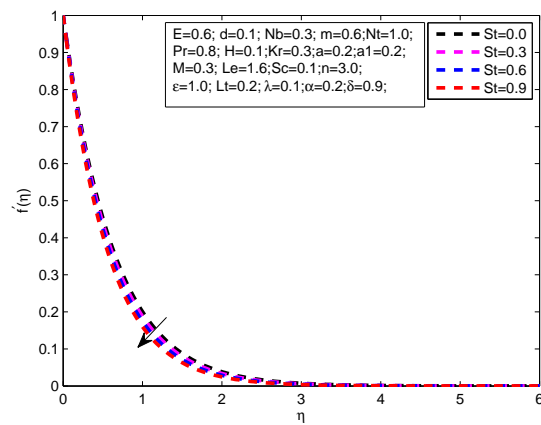


Figure 2. Distribution of f' for distinct values of St .

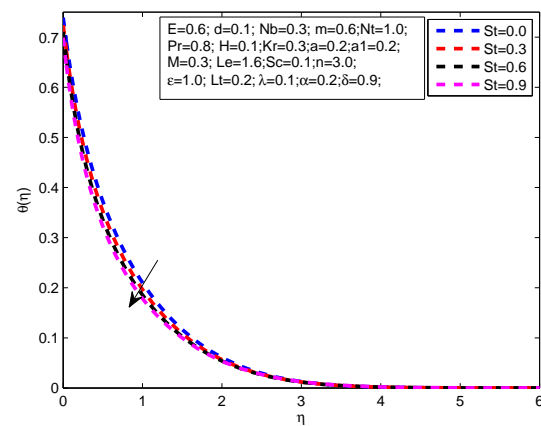


Figure 3. The f' and θ for distinct values of St .

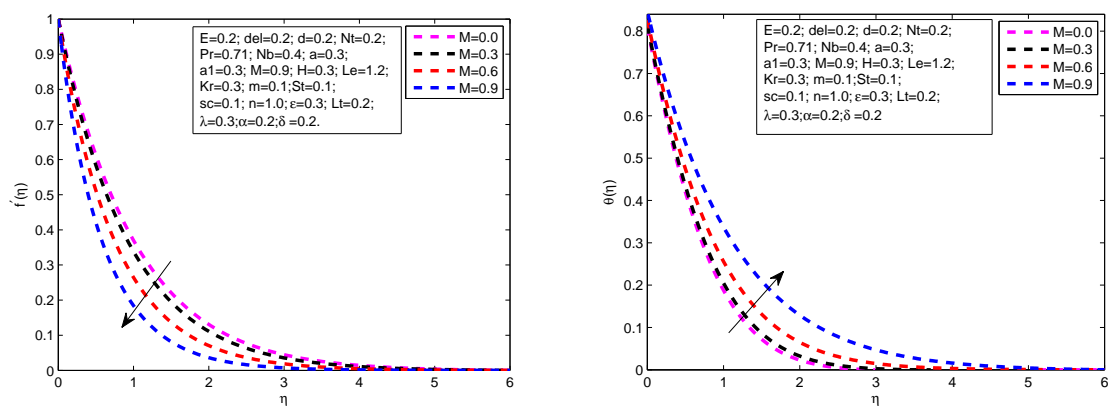


Figure 4. Variation of f' and θ for distinct values of M .

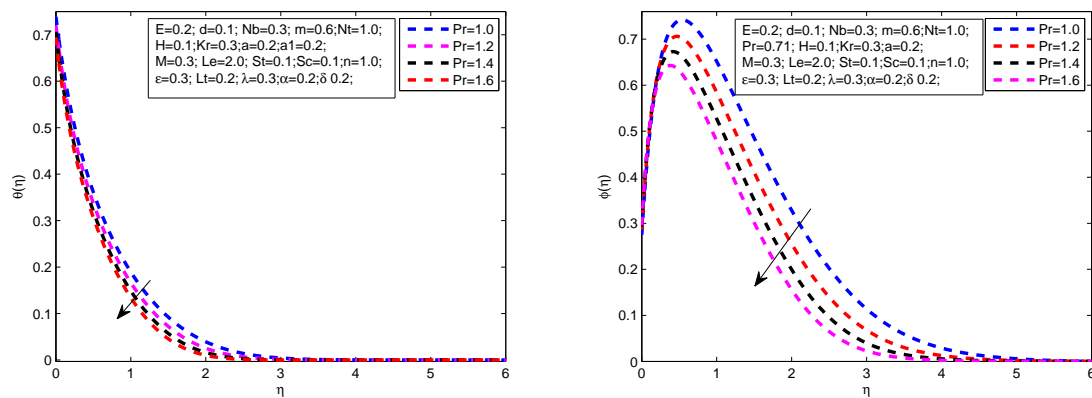


Figure 5. Variation of θ and ϕ .

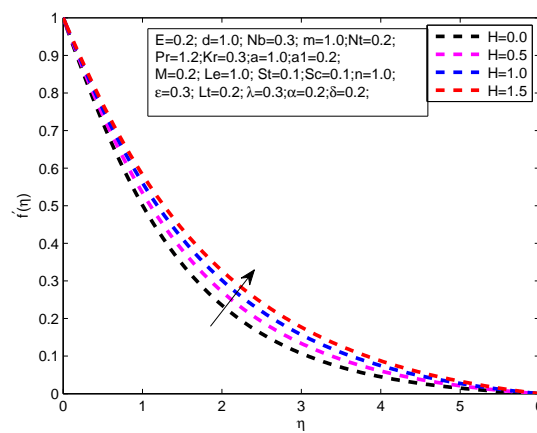


Figure 6. The behaviour of H on f' .

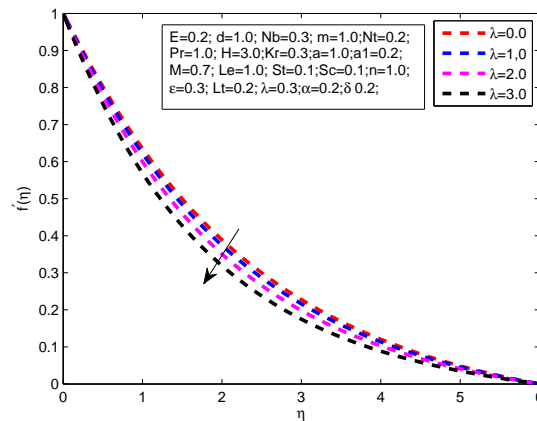


Figure 7. The behaviour of λ on f' .

Table 1. Comparison of $-f''(0)$ at $H = 1.0, m = \beta = St = a = \lambda = \zeta = 0$. for distinct values of M with perviously published data.

M	Akbar et al. [41]	Malik [42]	Hussain [43]	Rehman et al. [44]	Present Result
0.0	-1	-1	-1	-1	-1
0.5	-1.1180	-1.11802	-1.1180	-1.1180	-1.1180
1.0	-1.41421	-1.41419	-1.4137	-1.4142	-1.4141
5.0	-2.44949	-2.44945	-2.4495	-2.4495	-2.4497

Figure 7 demonstrated for velocity profile for unlike values of λ parameter. It is seen that the variation is enhancing λ is to increase both the film thickness and the free surface velocity $f'(\eta)$. The distribution of velocity profile for power law index m is shown in Figure 8. Decreases momentum and velocity boundary layer thickness by improving values of m . Here $m = 1$ linear represent the surface case and $m \neq 1$ corresponds to nonlinear stretching surface. Figure 9 exhibits the variation of m on the temperature field. It is noticed the temperature profile reduces by enhancing values of m . Figure 10 designates for the distribution of the concentration profile for various values of Le . The results shows that decreases in concentration profile is noticed for large valves of Lewis number Le . This is because of the fact that there is a reduction in the nano-particle volume fraction boundary layer thickness with the raise in the Lewis number. The variation of the concentration profile for the distinct values of Nb shown in Figure 11. It is noticed that reduction in concentration profile noticed by incrementing value of Brownian motion Nb . The effect of Nt on the concentration shown in Figure 12. It is seen that the concentration decreases as the thermosteresis parameter increases. Figure 13 is plotted to represents the variation (activation energy E) on concentration field ϕ . it is concluded that E is diminishing function of ϕ . The results shows that increases in concentration profile is noticed for large valves of E . Figure 14 designates for the distribution of the concentration profile for various values of (Lewis number Le). The results shows that decreases in concentration profile is noticed for large valves of Le . This is because of the fact that there is a reduction in the nano-particle volume fraction boundary layer thickness with the raise in the Lewis number. Figure 15 indicates the variation of concentration profile for the chemical reaction parameter Kr . The result has shown that concentration profile reduces by enhancing the values of Kr , a decreases in concentration is observed with increasing values of Kr . Figure 16 designates the temperature profile for the unlike values of the (Brownian motion parameters Nb). The result has shown that temperature distribution reduces by incrementing values of Nb . Figure 17 represents the distribution of the temperature profile for the various values of the Nt . The result has shown that temperature profile decreases by increasing values of thermophoresis Nt . The impact of (wall thickness parameter α) on velocity gradient is plotted in Figure 18. It is found that the velocity profile is increases for higher values of α . Figure 19 represents the effects of and fitted rate constant n on the nano-particle volume fraction. The antiparticles volume fraction profile decreases with an increasing value of fitted rate constant n which leads to considerable thinning with in the boundary layer. Figure 20 is plotted to represent the distribution of concentration profile for (temperature difference parameter δ). The result has shown that concentration profile is reduces by improving values of δ . Figure 21 is the distribution of temperature profile for different values of (variable thermal conductivity ϵ). The temperature profile increases by increasing values of ϵ . Figure 22 is plotted for the distinction of the temperature profile for the different values thermal slip parameter Lt The result has shown that the temperature profile increases by increasing value of Lt . Figure 23 is plotted for the impact of thickness parameter d on velocity gradient. For steps up values of thickness parameter d the velocity distribution enhances.

Next we calculate the numerical variation for different physical parameters through tables. Tables 2 and 3 are calculated to show the numerical aspects of skin fraction, Nusselt and Sherwood numbers for unlike values of different physical parameter. Tables 2 and 3 shows that the skin friction behavior increases for unlike values of M , m , β , St and λ . Skin friction steps down by the incrementing values of H , d (is shown in Tables 2 and 3). Nu_x increases with an increase in d , Lt , M , Pr and St . Nu_x steps down by increasing values of ϵ , m and R . Sherwood number Sh_x enhancement by steps up values of ζ , and Kr . Sherwood numbers Sh_x reduces by enlarging values of M , δ , Pr , E , m and Lc .

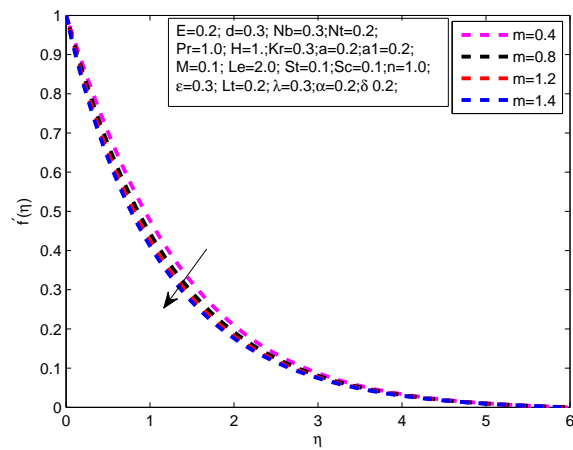


Figure 8. Influence of m on f' .

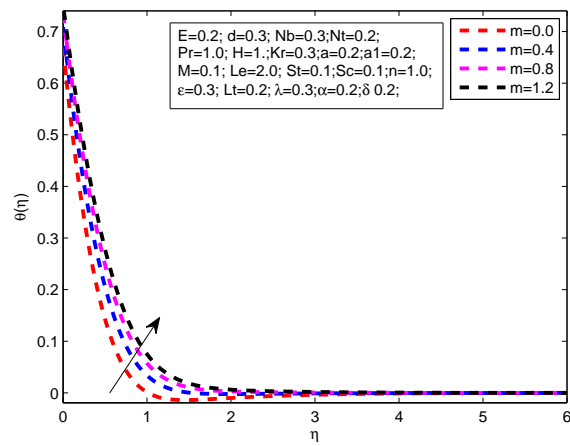


Figure 9. Variation of θ .

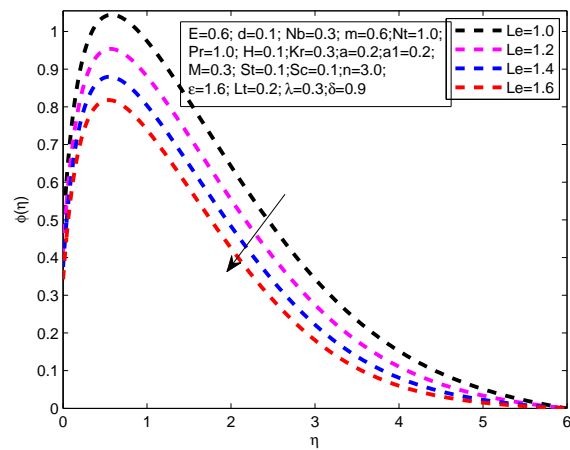


Figure 10. Variation of ϕ for distinct values of Le .

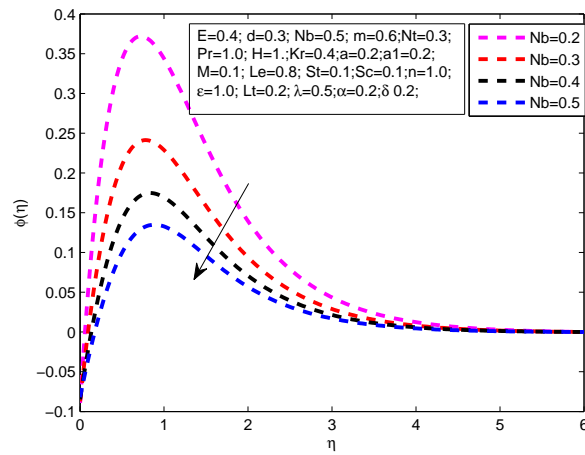


Figure 11. Variation of ϕ for distinct values of Nb .

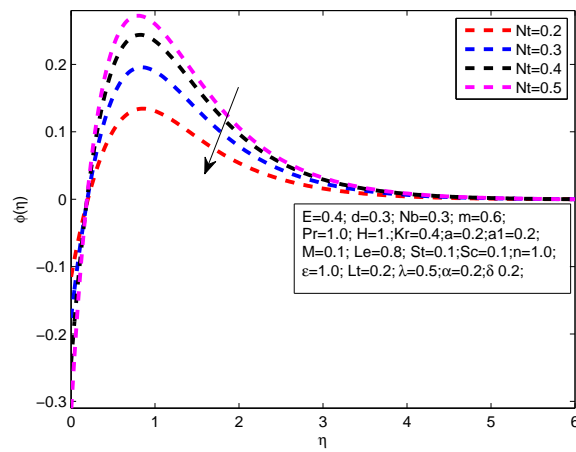


Figure 12. Variation of ϕ for distinct values of Nt .

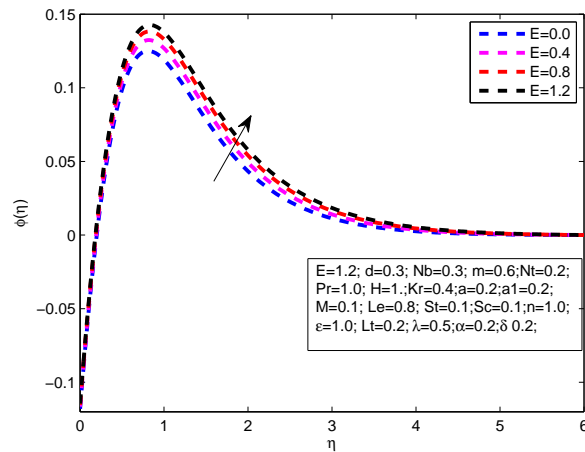


Figure 13. Variation of ϕ for distinct values of E .

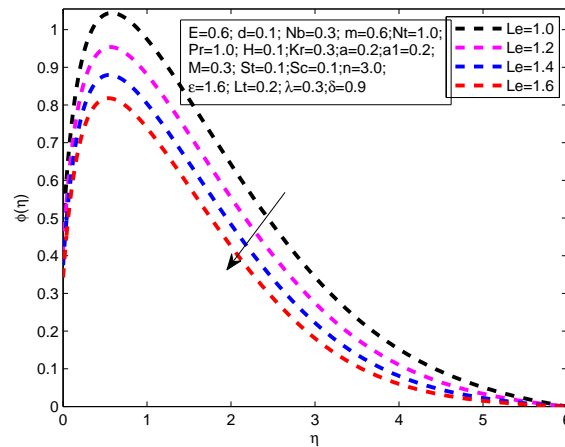


Figure 14. Variation of ϕ for distinct values of Le .

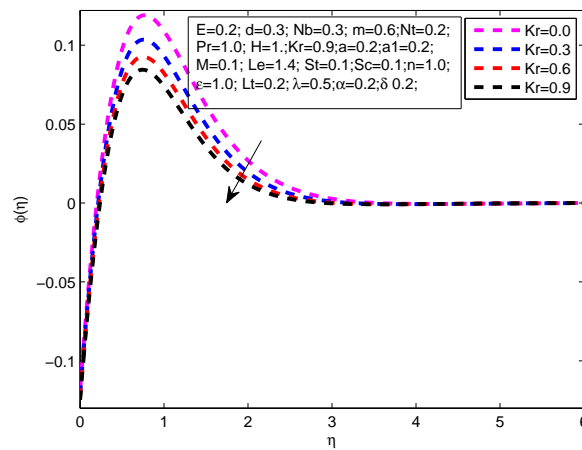


Figure 15. Variation of f' .

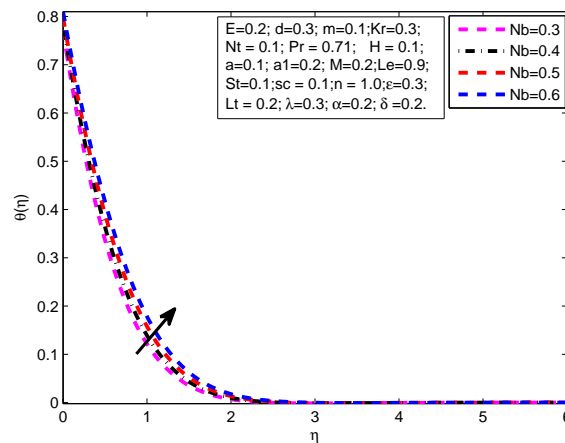


Figure 16. The behaviour of Nb on θ .

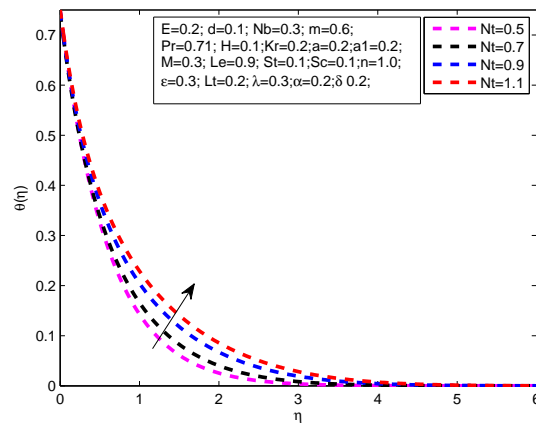


Figure 17. Influence of Nt on θ .

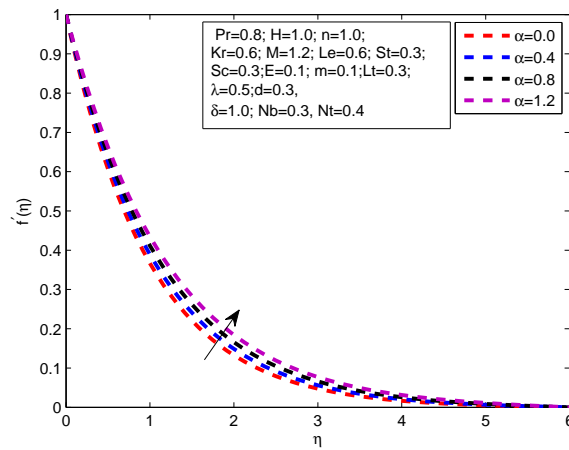


Figure 18. Variation of f' for distinct values of α .

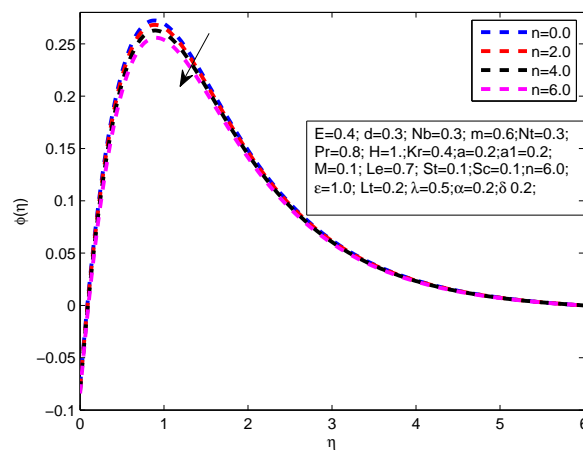


Figure 19. Variation of ϕ for distinct values of n .

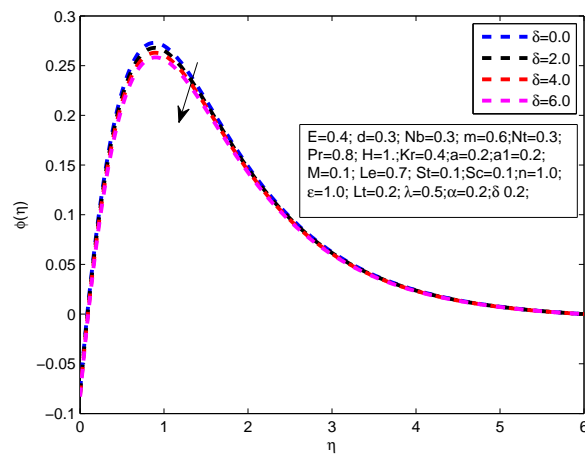


Figure 20. Variation of ϕ for distinct values of δ .

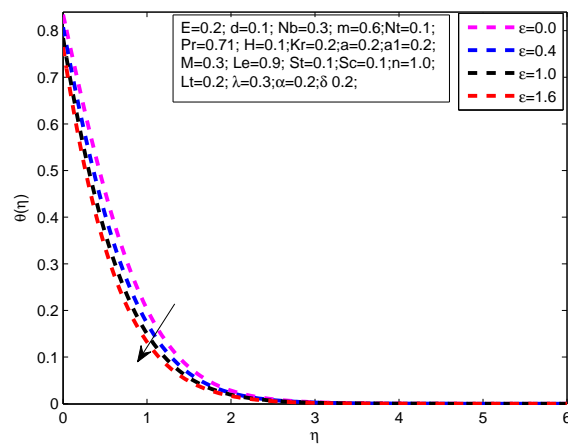


Figure 21. Variation of θ for distinct values of ϵ .

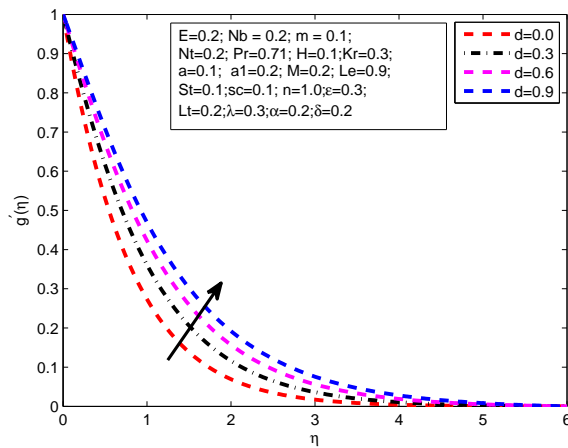


Figure 22. Variation of momentum profile for distinct values of d .

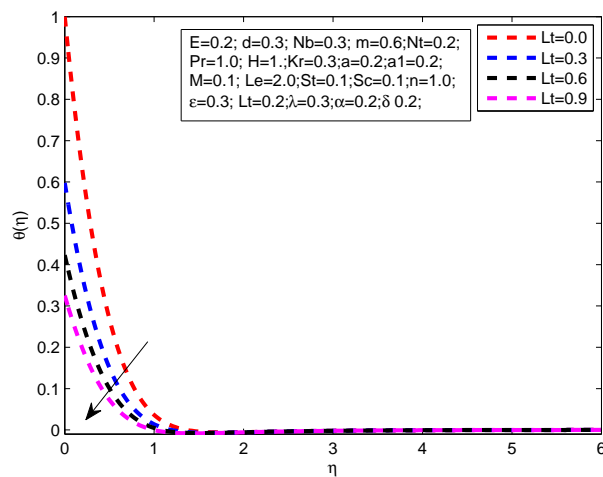


Figure 23. The temperature profile for distinct values of Lt .

Table 2. Effects of $A, M, Pr, \lambda, \varepsilon, Y, \delta$, and β on $-f''(0), -\theta'(0)$ and $-\phi'(0)$.

ξ	M	Pr	E	λ	St	ε	Y	β	m	δ	R	Kr	Dt	Lt	$-f''(0)$	$-\theta'(0)$	$-\phi'(0)$
1	1.2	0.8	0.4	0.3	0.5	0.3	1.0	90	0.0	0.4	0.7	0.5	0.3	0.6	0.7622	0.5753	0.6718
															1.1116	0.2136	0.1957
															1.0340	0.2157	0.1961
															0.9713	0.2178	0.1965
	0.0														0.5419	0.5436	0.6598
	0.3														0.6317	0.5655	0.6571
	0.6														0.7429	0.5880	0.6497
		0.75													0.5945	0.4833	0.6567
		1.0													0.5938	0.6452	0.5350
		1.3													0.6843	0.7643	0.4534
			0.0												0.8331	0.1892	0.2332
			0.2												0.6327	0.4780	0.2311
			0.4												0.5237	0.3893	0.2291
				0.0											0.5701	0.4863	0.6588
				0.3											0.5729	0.4859	0.6587
				0.6											0.5748	0.4845	0.6578
					0.0										0.8056	0.1520	0.2308
					0.2										0.8236	0.1765	0.2297
					0.4										0.8494	0.1892	0.2291
						0.0									0.6580	0.5769	0.6515
						0.3									0.6605	0.5760	0.6517
						0.6									0.6785	0.5729	0.6524

Table 3. Effects of $A, M, Pr, \lambda, \varepsilon, Y, \delta,$ and β on $-f''(0), -\theta'(0)$ and $-\phi'(0)$.

ζ	M	Pr	E	λ	St	ε	Y	β	m	δ	R	Kr	Dt	Lt	$-f''(0)$	$-\theta'(0)$	$-\phi'(0)$
1	1.2	0.8	0.4	0.3	0.5	0.3	1.0	90	0.0	0.4	0.7	0.5	0.3	0.6	0.7622	0.5753	0.6718
									0.0						0.9763	0.1810	0.2260
									0.3						0.9778	0.1787	0.2261
									0.6						0.9797	0.1760	0.2261
								0.0							0.9539	0.1781	0.2266
								45							0.9797	0.1760	0.2261
								90							1.0457	0.1739	0.2256
									0.0						0.9539	0.1801	0.2334
									0.2						0.9684	0.1719	0.2193
									0.4						0.9515	0.1638	0.2071
										0.0					0.9515	0.1638	0.2016
										0.2					0.9515	0.1638	0.2032
										0.4					0.9515	0.1638	0.2049
											0.0				0.9985	0.1778	0.2278
											0.2				0.9987	0.1746	0.2291
											0.4				0.9996	0.1731	0.2299
												0.0			0.9705	0.1632	0.2015
												0.3			0.9705	0.1632	0.2017
												0.6			0.9705	0.1632	0.2019
													0.0		0.9505	0.1638	0.1638
													0.3		0.9505	0.1638	0.1548
													0.6		0.9505	0.1638	0.2409
														0.0	0.8338	0.0000	0.2032
														0.3	0.9515	0.1638	0.2032
														0.6	1.0126	0.2055	0.2032

5. Conclusions

In this article we presents change in viscosity and temperature on incompressible flow of Eyring Powell nano-fluid in the attendance double stratification of induced by a non-linear stretching sheet. Moreover the effects of zero mass flux condition, activation energy and binary chemical reaction are taken into account. We use similarity transformation for the transforming nonlinear coupled ordinary differential equations. Successfully computed the solution of coupled ordinary differential equations via numerical scheme through shooting method followed by Runge-Kutta Fehlberg method. The behaviour of various parameters on velocity, temperature and concentration profiles are shown graphically. The behaviour of the local skin friction coefficient, local Nusselt number and local Sherwood number are shown numerically through table. The major conclusions are listed bellow.

- There is a decreases in velocity profile $f'(\eta)$ with increasing values of λ, m, St and M
- There is a increases in velocity profile $f'(\eta)$ with increasing values of H and α .
- The temperature profile increases $\theta(\eta)$ with the exceeding values of M, R, m, H, L, Nt and ε .
- Decrease in temperature $\theta(\eta)$ profile is noticed for the increasing values of Pr, St, Nb, n and M .
- The concentration profile $\phi(\eta)$ increments for large values of M, E and H .
- The concentration profile $\phi(\eta)$ reduces with the steps up values of Le, Kr, n, δ and Nb .

Author Contributions: Conceptualization, H.A.W. and H.Z.; methodology, S.B. and M.G.; software, S.K. and Y.N.; validation, H.A.W., H.Z., S.B., M.G., S.K., and Y.N.; funding acquisition, Y.N. All authors have read and agreed to the published version of the manuscript.

Funding: This research was supported by the Bio & Medical Technology Development Program of the NRF funded by the Korean government, MSIP(NRF-2015M3A9D7067219) and also supported by the Soonchunhyang University Research Fund.

Conflicts of Interest: The authors declare no conflict of interest.

Nomenclature

The following abbreviations and notations are used in this manuscript:

<i>ODE</i>	Ordinary Differential Equation	<i>MHD</i>	Magnatohydrodynamics
<i>BVP</i>	Boundary value problem	$k(\hat{T})$	Thermal conductivity
<i>IVP</i>	Initial value problem	k_∞	Free stream conductivity
<i>m</i>	Velocity power index parameter	K_r	Reaction rate parameter
α	Wall thickness parameter	μ	Temperature dependent viscosity parameter
<i>E</i>	Activation energy	<i>n</i>	Fitted rate constants
C_f	Local skin friction	λ, H	Fluid parameters
C_p	Specific heat	δ	Temperature relative parameter
<i>g</i>	Dimensionless velocity	<i>St, Sc</i>	stratification parameters
w_m	Local wall couple stress	<i>Nb</i>	Brownian motion parameter
Nu_x	Local Nusselt number	<i>Nt</i>	Thermophoresis parameter
<i>Pr</i>	Prandtl number	<i>Le</i>	Lewis number
<i>Kr</i>	Reaction rate parameter	L_t	Thermal Slip parameter
q_w	Wall heat flux	<i>M</i>	Magnetic parameter
Sh_x	Sherwood number	η	Plate surface
<i>Re</i>	Reynolds number	ε	Variable thermal conductivity
τ	Thermo-phoretic parameter	<i>d</i>	Temperature dependent viscosity parameter
\hat{T}_∞	Ambient temperature	\hat{T}_w	Wall temperature
<i>u</i>	Velocity component in <i>x</i> -direction	<i>v</i>	Velocity component in <i>y</i> -direction
μ	Viscosity	B_0	Magnetic induction
ζ	Boltzmann constant		

References

1. Sakiadis, B. Boundary-Layer Behavior on Continuous Solid Surfaces: II. The Boundary Layer on a Continuous Flat Surface. *AIChE J.* **1961**, *7*, 221–225. [[CrossRef](#)]
2. Vleggaar, J. Laminar boundary-layer behaviour on continuous, accelerating surfaces. *Chem. Eng. Sci.* **1977**, *32*, 1517–1525. [[CrossRef](#)]
3. Mabood, F.; Ibrahim, S.M.; Rashidi, M.M.; Shadloo, M.S.; Lorenzini, G. Non-uniform heat source/sink and Soret effects on MHD non-Darcian convective flow past a stretching sheet in a micropolar fluid with radiation. *Int. J. Heat Mass Transf.* **2016**, *93*, 674–682. [[CrossRef](#)]
4. Crane, L.J. Flow past a stretching plate. *Z. Angew. Math. Phys.* **1970**, *21*, 645–647. [[CrossRef](#)]
5. Haritha, A.; Devasena, Y.; Vishali, B. MHD Heat and Mass Transfer of the Unsteady Flow of a Maxwell Fluid over a Stretching Surface with Navier Slip and Convective Boundary Conditions. *Glob. J. Pure Appl. Math.* **2017**, *13*, 2169–2179. [[CrossRef](#)]
6. Zeb, H.; Wahab, H.A.; Shahzad, M.; Bhatti, S.; Gulistan, M. Thermal Effects on MHD Unsteady Newtonian Fluid Flow Over a Stretching Sheet. *J. Nanofluids* **2018**, *7*, 704–710. [[CrossRef](#)]
7. Zeb, H.; Wahab, H.A.; Shahzad, M.; Bhatti, S.; Gulistan, M. A Numerical Approach for the Thermal Radiation on MHD Unsteady Newtonian Fluid Flow Over a Stretching Sheet with Variable Thermal Conductivity and Partial Slip Conditions. *J. Nanofluids* **2018**, *7*, 870–878. [[CrossRef](#)]
8. Ghahderijani, M.J.; Esmaeili, M.; Afr, M.; Karimipour, A. Numerical Simulation of MHD Fluid Flow inside Constricted Channels using Lattice Boltzmann Method. *J. Appl. Fluid Mech.* **2017**, *10*, 1639–1648. [[CrossRef](#)]

9. Karimipour, A.; Taghipour, A.; Malvandi, A. Developing the laminar MHD forced convection flow of water or FMWNT carbon nanotubes in a microchannel imposed the uniform heat flux. *J. Magn. Magn. Mater.* **2016**, *419*, 420–428. [[CrossRef](#)]
10. Maleki, H.; Safaei, M.R.; Togun, H.; Dahari, M. Heat transfer and fluid flow of pseudo-plastic nanofluid over a moving permeable plate with viscous dissipation and heat absorption/generation. *J. Therm. Anal. Calorim.* **2019**, *135*, 1643–1654. [[CrossRef](#)]
11. Madhu, M.; Kishan, N.; Chamkha, A.J. Unsteady flow of a Maxwell nanofluid over a stretching surface in the presence of magnetohydrodynamic and thermal radiation effects. *Propuls. Power Res.* **2017**, *6*, 31–40. [[CrossRef](#)]
12. Kudenatti, R.; Kirsur, S.; Achala, L.; Bujurke, N. Exact solution of two-dimensional MHD boundary layer flow over a semi-infinite flat plate. *Commun. Nonlinear Sci. Numer. Simul.* **2017**, *18*, 1151–1161. [[CrossRef](#)]
13. Jamalabadi, M.Y.A.; Ghasemi, M.; Alamian, R.; Wongwises, S.; Afrand, M.; Shadloo, M.S. Modeling of Subcooled Flow Boiling with Nanoparticles under the Influence of a Magnetic Field. *Symmetry* **2019**, *11*, 1275. [[CrossRef](#)]
14. El-Dabe, N.; Ghaly, A.; Rizkallah, R.; Ewis, K.; Al-Bareda, A. Numerical solution of MHD boundary layer flow of non-newtonian casson fluid on a moving wedge with heat and mass transfer and induced magnetic field. *J. Appl. Math. Phys.* **2015**, *3*, 649–663. [[CrossRef](#)]
15. Khan, M.; Karim, I.; Islam, M.; Wahiduzzaman, M. MHD boundary layer radiative, heat generating and chemical reacting flow past a wedge moving in a nanofluid. *Nano Converg.* **2014**, *1*, 20–28. [[CrossRef](#)] [[PubMed](#)]
16. Malvandi, A.; Safaei, M.R.; Kaffash, M.H.; Ganji, D.D. MHD mixed convection in a vertical annulus filled with Al_2O_3 –water nanofluid considering nanoparticle emigration. *J. Magn. Magn. Mater.* **2015**, *82*, 296–306. [[CrossRef](#)]
17. Forghani-Tehrani, P.; Karimipour, A.; Afrand, M.; Mousavi, S. Different nano-particles volume fraction and Hartmann number effects on flow and heat transfer of water-silver nanofluid under the variable heat flux. *Phys. E Low-Dimens. Syst. Nanostruct.* **2017**, *85*, 271–279. [[CrossRef](#)]
18. Wahab, H.A.; Zeb, H.; Bhatti, S.; Gulistan, M.; Ahmad, S. A Numerical Approach of Slip Conditions Effect on Nanofluid Flow over a Stretching Sheet under Heating Joule Effect. *J. Math.* **2019**, *51*, 79–95.
19. Angayarkanni, A.; Sunny, V.; Philip, J. Effect of Nanoparticle Size, Morphology and Concentration on Specific Heat Capacity and Thermal Conductivity of Nanofluids. *J. Nanofluids* **2015**, *4*, 302–309. [[CrossRef](#)]
20. Hua, H.; Su, X. Unsteady MHD boundary layer flow and heat transfer over the stretching sheets submerged in a moving fluid with Ohmic heating and frictional heating. *Open Phys.* **2015**, *13*, 210–217. [[CrossRef](#)]
21. Maleki, H.; Safaei, M.R.; Alrashed, A.A.; Kasaeian, A. Flow and heat transfer in non-Newtonian nanofluids over porous surfaces. *J. Therm. Anal. Calorim.* **2019**, *135*, 1655–1666. [[CrossRef](#)]
22. Philip, J.; Angayarkanni, A. Tunable Thermal Transport in Phase Change Materials Using Inverse Micellar Templating and Nanofillers. *J. Phys. Chem. C* **2014**, *118*, 13972–13980. [[CrossRef](#)]
23. Lu, D.; Ramzan, P.D.M.; Huda, N.; Chung, J.; Farooq, U. Nonlinear radiation effect on MHD Carreau nanofluid flow over a radially stretching surface with zero mass flux at the surface. *Sci. Rep.* **2018**, *8*, 3709. [[CrossRef](#)] [[PubMed](#)]
24. Hayat, T.; Awais, M.; Asghar, S. Radiative effects in a three-dimensional flow of MHD Eyring-Powell fluid. *J. Egypt. Math. Soc.* **2013**, *21*, 379–384. [[CrossRef](#)]
25. Palumbo, F.; Main, I.; Zito, G. The thermal evolution of sedimentary basins and its effect on the maturation of hydrocarbons. *Geophys. J. Int.* **2002**, *139*, 248–260. [[CrossRef](#)]
26. Akbar, N. MHD Eyring-Prandtl fluid flow with convective boundary conditions in small intestines. *Int. J. Biomath.* **2013**, *6*, 1350034. [[CrossRef](#)]
27. Hayat, T.; Saif, R.S.; Muhammad, T.; Alsaedi, A.; Ellahi, R. On MHD nonlinear stretching flow of Powell-Eyring nanomaterial. *Results Phys.* **2017**, *7*, 535–543. [[CrossRef](#)]
28. Salahuddin, T.; Malik, M.; Hussain, A.; Bilal, S.; Awais, M. MHD flow of Cattaneo-Christov heat flux model for Williamson fluid over a stretching sheet with variable thickness: Using numerical approach. *J. Magn. Magn. Mater.* **2015**, *401*, 991–997. [[CrossRef](#)]
29. Hayat, T.; Khan, M.; Farooq, M.; Waqas, M.; Alsaedi, A.; Yasmeen, T. Impact of Cattaneo-Christov heat flux model in flow of variable thermal conductivity fluid over a variable thicked surface. *Int. J. Heat Mass Transf.* **2016**, *99*, 702–710. [[CrossRef](#)]

30. Bestman, A. Natural convection boundary layer with suction and mass transfer in a porous medium. *Int. J. Energy Res.* **1990**, *14*, 389–396. [[CrossRef](#)]
31. Awad, F.; Motsa, S.; Khumalo, M. Heat and Mass Transfer in Unsteady Rotating Fluid Flow with Binary Chemical Reaction and Activation Energy. *PLoS ONE* **2014**, *9*, e107622. [[CrossRef](#)] [[PubMed](#)]
32. Shafique, Z.; Mustafa, M.; Mushtaq, A. Boundary layer flow of Maxwell fluid in rotating frame with binary chemical reaction and activation energy. *Results Phys.* **2016**, *6*, 627–633. [[CrossRef](#)]
33. Abbas, Z.; Sheikh, M.; Motsa, S. Numerical solution of binary chemical reaction on stagnation point flow of Casson fluid over a stretching/shrinking sheet with thermal radiation. *Energy* **2016**, *95*, 12–20. [[CrossRef](#)]
34. Daniel, Y.; Aziz, Z.; Ismail, Z.; Salah, F. Thermal stratification effects on MHD radiative flow of nanofluid over nonlinear stretching sheet with variable thickness. *J. Comput. Des. Eng.* **2017**, *5*, 232–242. [[CrossRef](#)]
35. Mustafa, M.; Khan, J.; Hayat, T.; Alsaedi, A. Buoyancy effects on the MHD nanofluid flow past a vertical surface with chemical reaction and activation energy. *Int. J. Heat Mass Transf.* **2017**, *108*, 1340–1346. [[CrossRef](#)]
36. Mukhopadhyay, S. MHD boundary layer flow and heat transfer over an exponentially stretching sheet embedded in a thermally stratified medium. *Alex. Eng. J.* **2013**, *52*, 259–265. [[CrossRef](#)]
37. Ajayi, T.M.; Omowaye, A.J.; Animasaun, I.L. Effects of Viscous Dissipation and Double Stratification on MHD Casson Fluid Flow over a Surface with Variable Thickness: Boundary Layer Analysis. *Int. J. Eng. Res. Afr.* **2017**, *28*, 73–89. [[CrossRef](#)]
38. Daniel, Y.; Aziz, Z.; Ismail, Z.; Salah, F. Effects of thermal radiation, viscous and Joule heating on electrical MHD Nanofluid with double stratification. *Chin. J. Phys.* **2017**, *55*, 630–651. [[CrossRef](#)]
39. Khan, M.; Salahuddin, T.; Malik, M.; Mallawi, F. Change in viscosity of Williamson nanofluid flow due to thermal and solutal stratification. *Int. J. Heat Mass Transf.* **2018**, *126*, 941–948. [[CrossRef](#)]
40. Tencer, M.; Moss, J.S.; Zapach, T. Arrhenius average temperature: The effective temperature for non-fatigue wearout and long term reliability in variable thermal conditions and climates. *IEEE Trans. Compon. Packag. Technol.* **2004**, *27*, 1–15. [[CrossRef](#)]
41. Akbar, N.S.; Ebaid, A.; Khan, Z.H. Numerical analysis of magnetic field effects on Eyring Powell fluid flow towards a stretching sheet. *J. Magn. Magn. Mater.* **2015**, *283*, 355–358. [[CrossRef](#)]
42. Hussain, A.; Malik, M.; Awais, M.; Salahuddin, T.; Bilal, S. Computational and physical aspects of MHD Prandtl Eyring fluid flow analysis over a stretching sheet. *Neural Comput. Appl.* **2019**, *31*, 425–433. [[CrossRef](#)]
43. Malik, M.; Salahuddin, T.; Hussain, A.; Bilal, S. MHD flow of tangent hyperbolic fluid over a stretching cylinder using Keller box method. *J. Magn. Magn. Mater.* **2015**, *395*, 271–276. [[CrossRef](#)]
44. Rehman, K.U.; Awais, M.; Hussain, A.; Kousar, N.; Malik, M.Y. Mathematical analysis on MHD Prandtl-Eyring nanofluid new mass flux conditions. *J. Math. Appl. Sci.* **2019**, *42*, 24–38. [[CrossRef](#)]



© 2020 by the authors. Licensee MDPI, Basel, Switzerland. This article is an open access article distributed under the terms and conditions of the Creative Commons Attribution (CC BY) license (<http://creativecommons.org/licenses/by/4.0/>).